Electronic Supplementary Material (ESI) for Nanoscale.
This journal is © The Royal Society of Chemistry 2018

First-principles simulation of local response in transition metal dichalcogenides under electron irradiation - supplementary information

Anthony Yoshimura, Michael Lamparski, Neerav Kharche, Vincent Meunier

1 Calculation of the temperature-dependent displacement cross section

As the energies of the incident electrons climb into the ∼100 keV range, relativistic effects must be considered in the calculation of the differential cross section for the scattering of electrons off a chalcogen nucleus. Ignoring the effects of spin, this can be approximately determined with the classical Rutherford cross section

$$\frac{d\sigma^R}{d\Omega} = \left(\frac{\hbar\alpha}{2|\mathbf{p}|\beta} \csc^2(\theta/2) \right)^2, \tag{S1}$$

where θ is the electron's angle of deflection in the center of mass (CM) frame of the two-body system. Meanwhile, $\alpha = (4\pi\epsilon_0)^{-1} Ze^2/\hbar c \sim Z/137$ is the fine structure constant, $\mathbf{p}$ is the electron's initial relativistic 3-momentum, and β the ratio of its velocity to the speed of light.

Mott derived an exact solution to the differential cross section that incorporates the effects of spin predicted by the Dirac equation.[1] This solution was then expanded to first order in α by McKinley and Feshbach[2]

$$\frac{d\sigma^M}{d\Omega} = \frac{d\sigma^R}{d\Omega} \left\{ 1 - \beta^2 \sin^2\left(\frac{\theta}{2}\right) + \pi\alpha\beta \sin\left(\frac{\theta}{2}\right) \left[1 - \sin\left(\frac{\theta}{2}\right) \right] \right\}. \tag{S2}$$

Equation (S2) is accurate for electrons scattering off the nuclei of lighter elements (Z<21), so that $\alpha \ll 1$. For heavier nuclei, it has been shown that equation (S1) provides a more adequate approximation.[3,4] Therefore, we use equation (S2) to calculate the differential cross section for electrons scattering off a S nucleus, and equation (S1) for those scattering off a Se nucleus.

For sufficiently large TEM energy, there exists some critical scattering angle θ_d above which enough energy is transferred to the nucleus to displace it. We

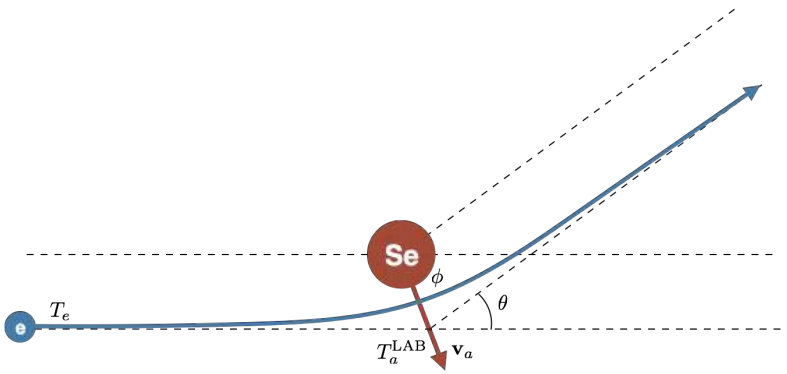

Figure S1: Schematic showing the scattering of an incident electron, and the resulting momentum transfer to a Se nucleus.

therefore define the displacement cross section as the cross section σ_0 for an electron scattering at an angle greater than or equal to θ_d

$$\sigma_0 = \sigma(\theta > \theta_d) = \begin{cases} 2\pi \int_{\theta_d}^{\pi} \frac{d\sigma^M(\theta)}{d\Omega} \sin(\theta) d\theta & \text{if } Z \leq 21 \\ 2\pi \int_{\theta_d}^{\pi} \frac{d\sigma^R(\theta)}{d\Omega} \sin(\theta) d\theta & \text{if } Z > 21 \end{cases} \tag{S3}$$

For $Z < 21$ we have

$$\begin{aligned} \sigma_0 = \frac{\pi\hbar^2\alpha^2}{|\mathbf{p}|^2\beta^2} \Bigg\{ \csc^2\left(\frac{\theta_d}{2}\right) - (\beta^2 + \pi\alpha\beta) \ln\left[\csc^2\left(\frac{\theta_d}{2}\right)\right] \\ + 2\pi\alpha\beta\left[\csc\left(\frac{\theta_d}{2}\right) - 1\right] - 1 \Bigg\}, \end{aligned} \tag{S4}$$

while for $Z \geq 21$

$$\sigma_0 = \frac{\pi\hbar^2\alpha^2}{|\mathbf{p}|^2\beta^2} \left\{ \csc^2\left(\frac{\theta_d}{2}\right) - 1 \right\}. \tag{S5}$$

We define the displacement threshold T_d as the minimum energy transfer required to displace the chalcogen. That is, T_d is the energy transferred when the scattering angle is θ_d. We wish to rewrite equations (S4) and (S5) in terms of T_d rather than θ_d, as the values of T_d can be found approximately as shown in table 2 in the main text.

If we assume that the mass of the nucleus M is much greater than that of the electron m, conservation of 4-momentum determines the energy transferred to the chalcogen nucleus T_a^{CM} in the CM frame as a function of the scattering angle[5]

$$T_a^{\mathrm{CM}} \sim T_m \sin^2\left(\frac{\theta}{2}\right), \qquad m \ll M, \tag{S6}$$

where

$$T_m \sim \frac{2T_e(T_e + 2m)}{M}, \qquad m \ll M, \tag{S7}$$

is the maximum amount of energy that can be transferred given the TEM energy T_e. Rearranging equation (S6) then gives

$$\csc^2\left(\frac{\theta_d}{2}\right) = \frac{T_m}{T_d}, \tag{S8}$$

which we can plug into (S3) to obtain the displacement cross section in terms of T_d as shown in equations (1) and (2) in the main text.

We are now ready to consider the effect of lattice vibrations on the displacement cross section. Equations (S1) and (S2) are given in the CM frame, in which the nucleus is approximately stationary before the scattering event. However, in the laboratory frame, in which the entire TMD crystal is stationary, the nucleus has non-zero initial velocity due to lattice vibrations. This can enhance or reduce the likelihood of displacement depending on the nucleus's speed and direction.

We can express the nucleus's total energy before the scattering event as $Mv_0^2/2$, where v_0 is its maximum velocity in the z-direction (choosing the positive z-directions as that of the incident electrons' velocity). Assuming that the vibrational motion is harmonic, we can write the potential and kinetic energy as

$$U_0 = \frac{Mv_0^2}{2}\sin^2(\omega t) \qquad \text{and} \qquad T_0 = \frac{Mv_0^2}{2}\cos^2(\omega t) \tag{S9}$$

respectively, where ω is the frequency of vibration.

If an electron is scattered at an angle θ, we know the transferred energy in the CM frame from the asymptotic formula (S6). Additionally, because the vibrational velocity of a chalcogen nucleus is much smaller than the speed of light, we can determine its velocity in the laboratory frame by a Galilean transformation. The total energy of the nucleus after the scattering event in the laboratory frame is then

$$\begin{aligned} E_{\text{tot}} &= T_a^{\text{LAB}} + U_0 \\ &= \frac{M}{2}[v_a^{\text{CM}} + v_0\cos(\omega t)]^2 + \frac{Mv_0^2}{2}\sin^2(\omega t). \end{aligned} \tag{S10}$$

Here v_a^{CM} is the final velocity of the chalcogen nucleus in the CM frame, obtained from (S6)

$$v_a^{\text{CM}} = \sin\left(\frac{\theta}{2}\right)\sqrt{\frac{2T_m}{M}}. \tag{S11}$$

We note that, because the LAB frame velocity of the electron is much greater than that of the nucleus, both the TEM energy T_e scattering angle θ are essentially unchanged when switching from the CM to the LAB frame. It follows that T_m given in the asymptotic formula (S7) holds in either frame.

Inserting equation (S11) into (S10) gives the total energy of the nucleus as a function of θ

$$E_{\text{tot}} = \frac{M}{2}\left[\sin\left(\frac{\theta}{2}\right)\sqrt{\frac{2T_m}{M}} + v_0\cos(\omega t)\right]^2 + \frac{Mv_0^2}{2}\cos^2(\omega t). \tag{S12}$$

At the onset of displacement, we set $E_{\text{tot}} = T_d$ and $\theta = \theta_d$. Then we can rearrange equation (S12) into the form of (S8).

$$\csc^2\left(\frac{\theta_d}{2}\right) = \frac{T_m}{\widetilde{T}_d}, \tag{S13}$$

where

$$\widetilde{T}_d(v_0, t, T_d) = T_d - U_0 + T_0 + v_0\cos(\omega t)\sqrt{2M(T_d - U_0)} \tag{S14}$$

can be thought of as the effective displacement threshold when considering vibrations. Inserting equation (S13) back into equation (S3) yields the displacement cross section as a function of v_0, t, and T_d.

To produce the plots in the main text, we found the expectation value of the displacement cross section by taking a weighted sum over the possible values of v_0 and then integrating over time. Treating a vibrating nucleus as a quantum harmonic oscillator, we can express its energy as

$$E_{\{n_{\mathbf{k},s}\}} = \sum_{\mathbf{k},s}\hbar\omega_{\mathbf{k},s}\left(n_{\mathbf{k},s} + \frac{1}{2}\right), \tag{S15}$$

where $\mathbf{k}$ is the phonon wave-vector and s labels the normal modes. The quantum number $n_{\mathbf{k},s}$ counts the number of excitations for a particular mode and wave-vector, and $\{n_{\mathbf{k},s}\}$ represents a set of possible excitations numbers. Boltzmann statistics determine the probability of finding the nucleus at particular energy [6]

$$P\left(E_{\{n_{\mathbf{k},s}\}}\right) = \frac{1}{Z}\exp\left\{-\frac{1}{k_BT}\sum_{\mathbf{k},s}\hbar\omega_{\mathbf{k},s}\left(n_{\mathbf{k},s} + \frac{1}{2}\right)\right\}, \tag{S16}$$

where k_B is the Boltzmann constant and T is the temperature. The partition function Z is given by

$$Z = \prod_{\mathbf{k},s}\frac{e^{\hbar\omega_{\mathbf{k},s}/2k_BT}}{e^{\hbar\omega_{\mathbf{k},s}/k_BT} - 1}. \tag{S17}$$

We need only consider modes in which the chalcogen oscillates in the direction perpendicular to the TMD plane. For a TMD monolayer in the H phase, these are the A_1' and the A_2'' modes. [7] The frequencies of these particular modes are close to one another and have a weak dependence on the wave-vector $\mathbf{k}$. Thus, it suffices to use only one frequency, that corresponding to $\mathbf{k} = 0$ for the A_1' mode, in the probability equation (S16). As the A_1' mode is Raman active, the

corresponding frequencies are well-documented for the group-IV TMDs,[8,9] and are listed in table 2 in the main text. Equation (S16) thus reduces to

$$P(n) = e^{-\hbar\omega n/k_B T}\left(1 - e^{-\hbar\omega/k_B T}\right), \tag{S18}$$

where we have removed the summation over $\mathbf{k}$ and s. Using $E_n = mv_n^2/2$, we can rearrange equation (S15) to solve for v_n

$$v_{n\pm} = \pm\sqrt{\frac{2\hbar\omega(n+1/2)}{M}}, \tag{S19}$$

where we note that $v_{n\pm}$ can be positive or negative for a given n. By inserting this into the effective displacement threshold (S14) as v_0, the displacement cross sections (S4) and (S5) become functions of n and t, so that $\sigma_0 = \sigma_0(v_{n\pm}, t)$.

The expectation value is determined by taking a weighted sum over n and averaging over t.

$$\sigma(T_e, T_d, T) = \frac{\omega}{\pi}\int_0^{\pi/2\omega} dt \sum_{n=0}^{\infty} P(n,T)\Big\{\sigma_0(v_{n+},t)\Theta(T_m(T_e) - \widetilde{T}_d(v_{n+},t,T_d)) + \sigma_0(v_{n-},t)\Theta(T_m(T_e) - \widetilde{T}_d(v_{n-},t,T_d))\Big\}. \tag{S20}$$

The inclusion of the Heaviside function $\Theta(T_m - \widetilde{T}_d)$ ensures that we only sum over normal modes for which the displacement can occur. Equation (S20) is equivalent to equation (4) in the main text, except that here, we explicitly show that both positive and negative velocities are accounted for. The summation is carried out up to $n = 50 * n_{\mathrm{BE}}(T)$, where

$$n_{\mathrm{BE}}(T) = \frac{1}{e^{\hbar\omega/kT} - 1} \tag{S21}$$

gives the expectation value of n according to Bose-Einstein statistics. Meanwhile, 10-point Gaussian quadrature is used to determine the integral over t.

2 Calculating the recoil angle

The asymptotic formula (5) in the main text gives the recoil angle of the chalcogen nucleus in the laboratory frame as a function of the energy transferred during the scattering event. The derivation of this relationship relies on conservation of 4-momentum, where the 4-momentum vector takes the form

$$p^\mu = (E, \mathbf{p}) = \left(\frac{m}{\sqrt{1-v^2}}, \frac{m\mathbf{v}}{\sqrt{1-v^2}} \right). \tag{S22}$$

For the electron-nucleus interaction, conservation of 4-momentum guarantees that

$$(p_e^i + p_a^i)^\mu = (p_e^f + p_a^f)^\mu, \tag{S23}$$

where electron and chalcogen atom momenta are denoted by the subscripts e and a, and the i and f superscripts indicate initial and final momenta. ϕ is the angle between the directions of the incident electron and the recoiled nucleus, as shown in figure S1. Therefore, to solve for ϕ, we start by bringing p_e^i and p_a^f to the same side of the equation,

$$(p_e^f - p_a^i)^\mu = (p_e^i - p_a^f)^\mu. \tag{S24}$$

We then take the inner product with the covariant vectors,

$$(p_e^f - p_a^i)_\mu (p_e^f - p_a^i)^\mu = (p_e^i - p_a^f)_\mu (p_e^i - p_a^f)^\mu. \tag{S25}$$

Noting that the inner product of a 4-momentum with itself is the square of the particle's mass, we have

$$m^2 + M^2 - 2(p_e^f)_\mu (p_a^i)^\mu = m^2 + M^2 - 2(p_e^i)_\mu (p_a^f)^\mu. \tag{S26}$$

After cancellation, we rewrite everything in terms of energy and 3-momentum.

$$E_e^f E_a^i - \mathbf{p}_e^f \cdot \mathbf{p}_a^i = E_e^i E_a^f - \mathbf{p}_e^i \cdot \mathbf{p}_a^f \tag{S27}$$

Let $\mathbf{u}_\gamma$ and $\mathbf{v}_\gamma$ denote initial and final velocities of particle γ. In the laboratory frame, $\mathbf{u}_a = 0$, so

$$\frac{mM}{\sqrt{1-v_e^2}} = \frac{mM}{\sqrt{1-u_e^2}\sqrt{1-v_a^2}} - \frac{mM\mathbf{u}_e \cdot \mathbf{v}_a}{\sqrt{1-u_e^2}\sqrt{1-v_a^2}}, \tag{S28}$$

which simplifies to

$$\frac{1}{\sqrt{1-v_e^2}} = \frac{1 - u_e v_a \cos\phi}{\sqrt{1-u_e^2}\sqrt{1-v_a^2}}. \tag{S29}$$

To eliminate v_e, we then employ conservation of energy

$$E_e^i + E_a^i = E_e^f + E_a^f, \tag{S30}$$

which equals

$$\frac{m}{\sqrt{1-u_e^2}} + M = \frac{m}{\sqrt{1-v_e^2}} + \frac{M}{\sqrt{1-v_a^2}}. \tag{S31}$$

Substituting equation (S29) into (S31) yields

$$\frac{m}{\sqrt{1-u_e^2}} + M = \frac{m(1-u_e v_a \cos\phi)}{\sqrt{1-u_e^2}\sqrt{1-v_a^2}} + \frac{M}{\sqrt{1-v_a^2}}. \tag{S32}$$

Assuming $v_a \ll 1$ and $m/M \ll 1$, we can expand the radicals containing v_a, so that

$$\begin{aligned} \frac{m}{M}\frac{1}{\sqrt{1-u_e^2}} + 1 &\sim \frac{m}{M}\left(\frac{1-u_e v_a \cos\phi}{\sqrt{1-u_e^2}}\right)\left(1+\frac{v_a^2}{2}\right) + \left(1+\frac{v_a^2}{2}\right) \\ &\sim \frac{m}{M}\left(\frac{1-u_e v_a \cos\phi}{\sqrt{1-u_e^2}}\right) + \left(1+\frac{v_a^2}{2}\right), \end{aligned} \tag{S33}$$

where in the second line, we neglect the term of order mv_a^2/M. After simplifying and rearranging, we arrive at.

$$\cos^2\phi \sim \left(\frac{Mv_a}{2m}\right)^2 \left(\frac{1-u_e^2}{u_e^2}\right). \tag{S34}$$

We can write the right side of the asymptotic formula (S34) in terms of the kinetic energies of the incident electron and recoiled chalcogen, given by

$$T_e = \frac{m}{\sqrt{1-u_e^2}} - m \qquad \text{and} \qquad T_a^{\mathrm{LAB}} = \frac{Mv_a^2}{2}. \tag{S35}$$

Finally, we use the maximum energy transfer T_m from formula (S7) to write

$$\cos^2\phi \sim \frac{T_a^{\mathrm{LAB}}}{T_m}. \tag{S36}$$

Table S1: Formation energies of various defects normalized per chalcogen vacancy, calculated using the LDA

	formation energy (eV)			
TMD	vacancy	divacancy	3DV cluster	trefoil
MoS_2	3.92	3.93	4.01	4.00
WS_2	4.16	4.04	4.06	4.10
$MoSe_2$	3.90	3.74	3.83	3.60
WSe_2	3.90	3.67	3.75	3.53

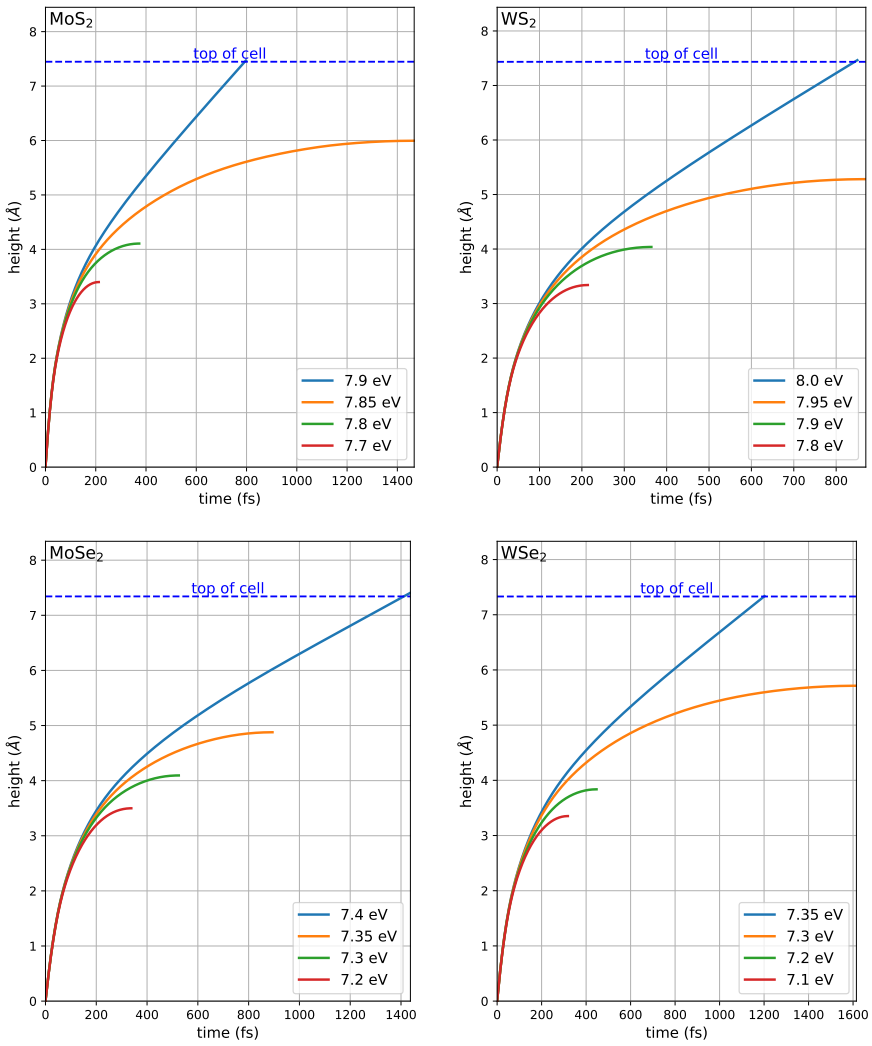

Figure S2: Chalcogen trajectories moving away from the TMD layer in molecular dynamics for various initial kinetic energies. Chalcogens start at their pristine positions and are shot away from the crystal with positive initial velocities corresponding to the kinetic energies indicated in the legend. Calculations stop if the chalcogen's velocity falls below zero. The calculated displacement threshold is the lowest kinetic energy for which the chalcogen reaches the top of the cell. To achieve a precision of 0.1 eV for each TMD, we run a sequence of calculations over of small range of initial velocities corresponding to intervals of 0.05 eV.

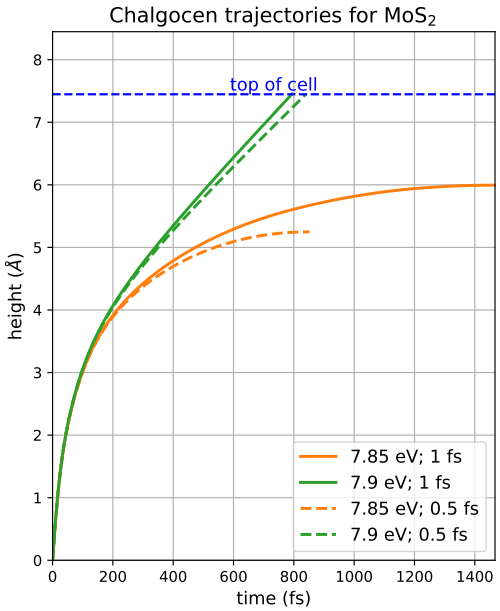

Figure S3: S trajectories moving away from an MoS_2 layer in molecular dynamics. The S atom starts at its pristine position and is shot away from the MoS_2 crystal with initial kinetic energies indicated in the legend. The solid curves correspond to simulations that employed a 1.0 fs time step, and are identical to the curves shown in supplementary figure S2. The dashed curves correspond to a 0.5 fs time step. 1.0 fs and 0.5 fs time steps produce very similar trajectories, in that both signify the same value for the displacement threshold within the desired precision of 0.1 eV. This demonstrates that a time step of 1.0 fs is sufficiently small for these simulations.

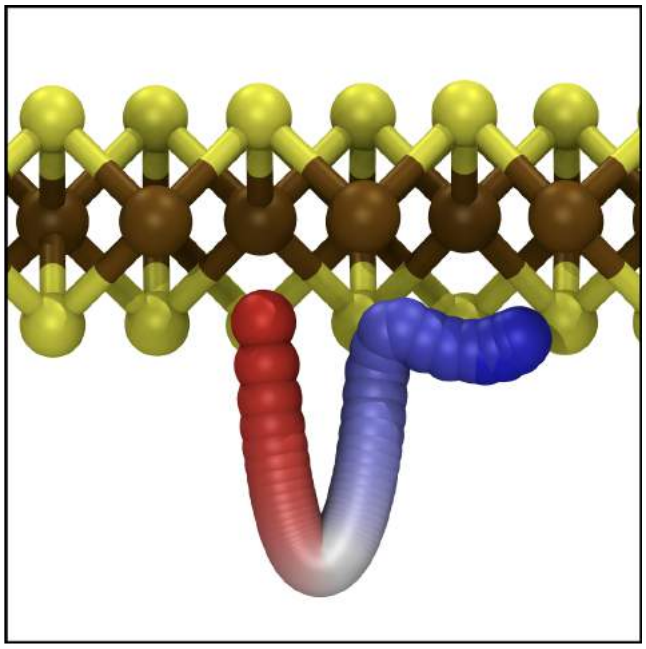

Figure S4: Trajectory of S migration in MoS_2 calculated using DFT-based MD for a TEM energy of 105 keV. Here the electron transfers 7.86 eV to the chalcogen nucleus, just below the 7.9 eV needed for sputtering. The color gradient for red to blue indicates the time evolution through 680 fs.

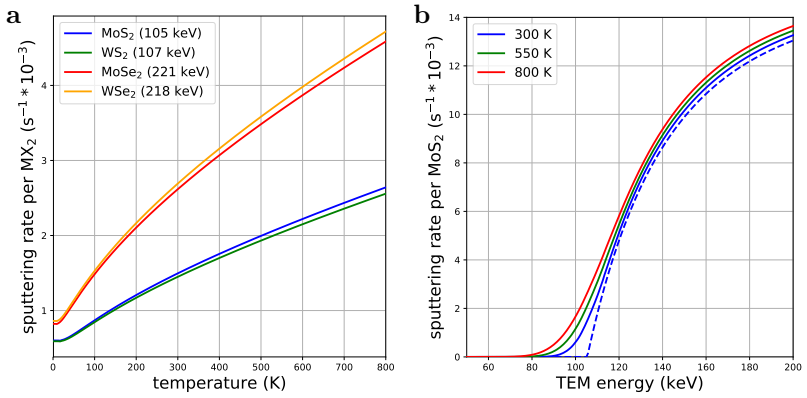

Figure S5: (a) Sputtering rate for all group-VI at their respective critical sputtering TEM energies with a current density of $1.3{\times}10^6$ e/nm^2/s. For temperatures hotter than room temperature, the sputtering rate increases approximately linearly with temperature. (b) Sputtering rate for MoS_2 at several temperatures under the same current density. The dashed curve shows the sputtering rates of a static crystal. The increase in rate brought on by thermal lattice vibrations is most pronounced at the critical energy.

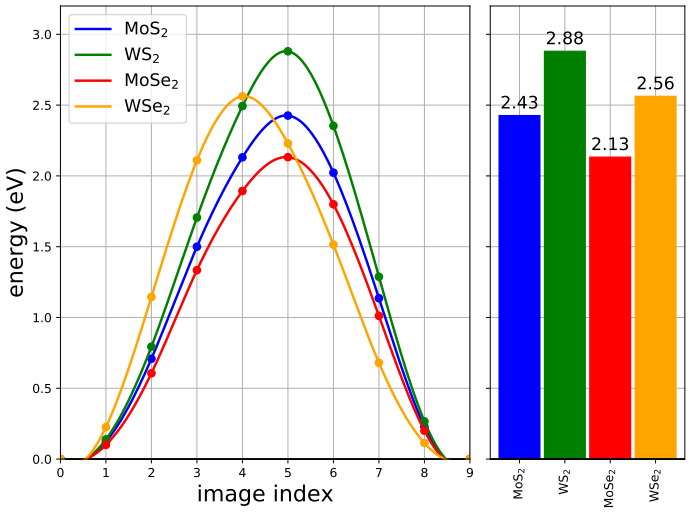

Figure S6: Energy profiles of isolated vacancy migrations for the four group-VI TMDs with cubic interpolation. The activation energies are shown in the bar chart on the right.

	○○	○●	●○	●●
○○○○	0.43	0.45	0.89	0.79
○○○●	0.55	0.56	1.01	0.80
○○●○	1.37	0.91	1.36	1.55
○○●●	1.47	1.45	2.02	1.69
○●○○	1.01	0.70	1.21	1.00
○●○●	0.65	0.91	2.14	1.26
○●●○	1.75	1.85	2.36	2.04
○●●●	2.20	1.88	2.46	2.11
●○○○	0.30	0.42	0.93	0.58
●○○●	0.56	0.52	1.03	0.58
●○●○	1.81	1.59	2.82	2.07
●○●●	2.02	1.77	2.35	1.93
●●○○	1.02	0.56	1.23	1.08
●●○●	0.56	0.79	1.48	2.52
●●●○	2.49	2.00	2.69	2.67
●●●●	2.72	2.26	2.96	2.56

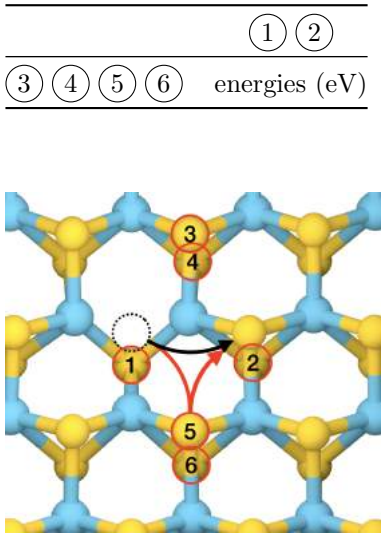

Figure S7: Migration activation energies corresponding to all 64 nearest-neighbor configurations in WSe_2, calculated using the NEB method and the LDA. The sets of filled and hollow circles along the top row and left column of the table specify which of the six neighboring chalcogen sites are occupied (e.g., a hollow circle indicates a vacant site). The key on the upper right show how the circles map to the locations of the sites, where the numbers encircled correspond to the sites labelled in the diagram on the lower right. Generally, the activation energies tend to decrease as the number of neighboring vacancies increases. Energies highlighted in red are exactly equivalent to the energy highlighted green. In these cases, the chalcogen follows the red path shown in the image, migrating first to vacant site-5 before hopping to the final site. The migration to site-5 is equivalent to the one corresponding to the green highlight.

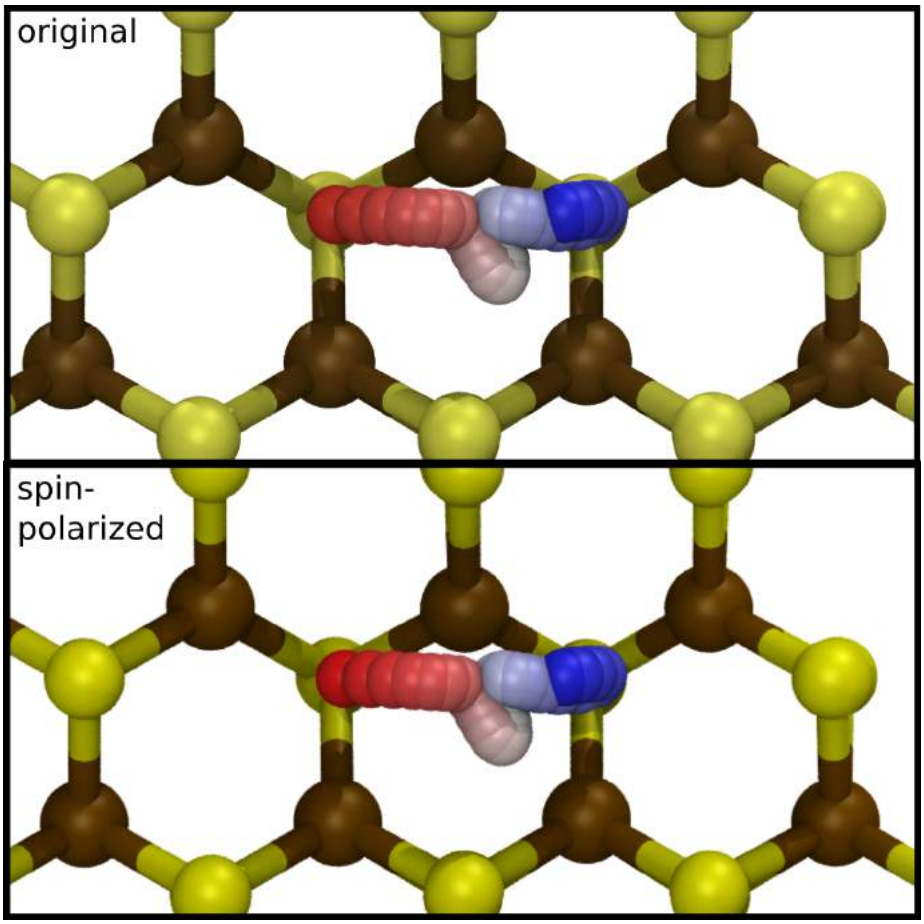

Figure S8: S migration in MoS_2 resulting from an energy transfer of 4.1 eV to the S atom. The top shows the simulated trajectory without accounting for spin polarization, as shown in figure 3a in the main text. The trajectory shown underneath allows for spin polarization. The difference in the trajectories is inperceptible, and thus, we do not account for spin polarization to obtain the displacement thresholds in the main text.

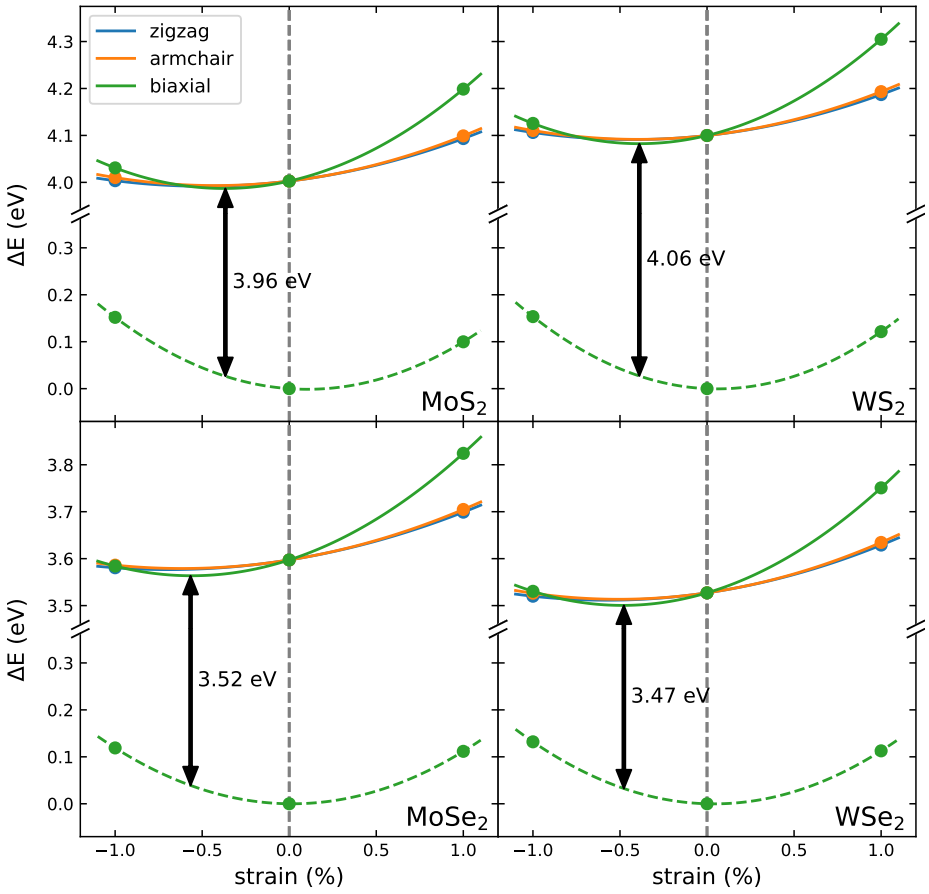

Figure S9: Formation energies of the trefoil defect in the four TMDs considered, under zigzag, armchair, and biaxial strain with parabolic fits. The change in free energy of pristine crystals under biaxial strain are plotted with dashed fits. 0% strain corresponds to the lattice constants of the pristine cell. All trefoil structures are most stable under slight biaxial compression relative to the pristine lattice parameters. This effect is more pronounced in the selenides. The double headed arrows indicate the formation energy at the compression that yields the lowest free energy for the trefoil structure. Comparing these energies to those in table S1, we see that slight compression lowers the formation energy by about 0.05 eV for the four TMDs.

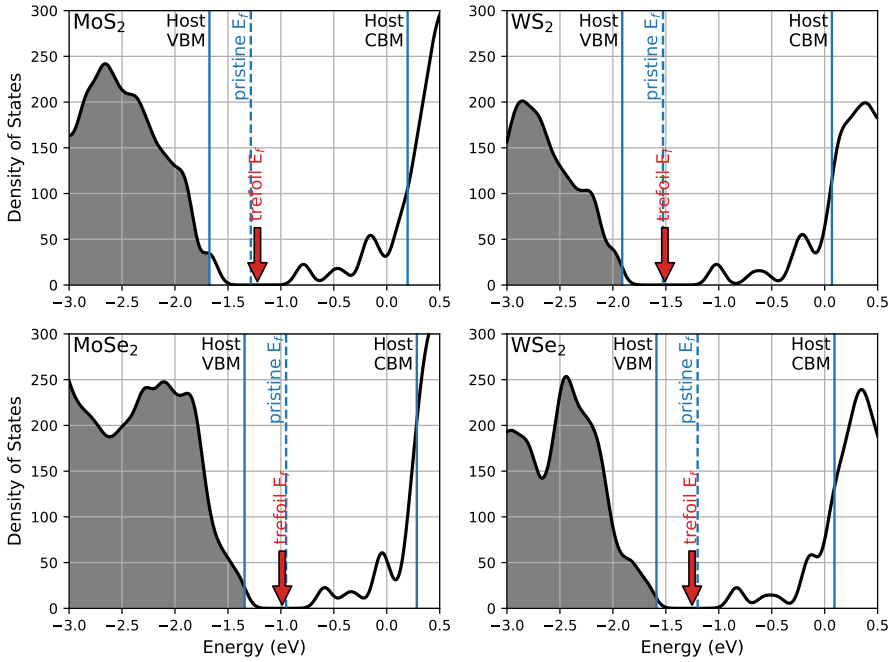

Figure S10: Density of states for all four TMDs with a trefoil defect. The band edges of the pristine materials are shown in solid blue lines, while the dashed lines mark the pristine Fermi levels. The red arrows indicate the Fermi level of the trefoil system. The presence of a trefoil produces several gap states inside of the pristine band gap.

References

[1] N. F. Mott, *Proc. Royal Soc. A*, 1929, **124**, 425–442.

[2] W. A. McKinley and H. Feshbach, *Phys. Rev.*, 1948, **74**, 1759–1763.

[3] R. F. Egerton, R. McLeod, F. Wang and M. Malac, *Ultramicroscopy*, 2010, **110**, 991–997.

[4] O. S. Oen, *Cross sections for atomic displacements in solids by fast electrons*, Oak ridge national laboratory technical report, 1973.

[5] G. S. Khandelwal and E. Merzbacher, *Phys. Rev.*, 1963, **130**, 1822–1825.

[6] N. W. Ashcroft and N. D. Mermin, *Solid State Physics*, Saunders College Publishing, 1976, p. 453.

[7] X. Zhang, X.-f. Qiao, W. Shi, J.-b. Wu, D.-s. Jiang and P.-h. Tan, *Chem. Soc. Rev.*, 2015, **44**, 2757–2785.

[8] L. Liang and V. Meunier, *Nanoscale*, 2014, **6**, 5394–401.

[9] H. Terrones, E. Del Corro, S. Feng, J. M. Poumirol, D. Rhodes, D. Smirnov, N. R. Pradhan, Z. Lin, M. a. T. Nguyen, a. L. Elías, T. E. Mallouk, L. Balicas, M. a. Pimenta and M. Terrones, *Sci. Rep.*, 2014, **4**, 4215.